Apoptosis (2025) 30:1042–1057
https://doi.org/10.1007/s10495-025-02078-0

Magea13 attenuates myocardial injury in acute myocardial infarction by inhibiting the cAMP-PKA signaling pathway

Jialin Zheng[1] · Xiaoyu Xu[1] · Ziwei Zhang[1] · Kanghui Ge[1] · Yi Xiang[1] · Hualei Dai[2]

Accepted: 10 January 2025 / Published online: 8 March 2025

Abstract

Object Acute myocardial infarction (AMI) is a serious cardiovascular disease for which there are still no effective therapeutic options available, and melanoma-associated antigen-A13 (Magea13), a member of the MAGE superfamily, has an unknown role in AMI. This study aims to investigate the potential role and molecular mechanisms of Magea13 in myocardial injury associated with AMI through in vivo and in vitro experiments.

Methods Firstly, differentially expressed genes (DEGs) and signaling pathways were screened by RNA sequencing. Cardiac-specific Magea13 overexpression was achieved with the adeno-associated virus type 9 serotype system. Subsequently, these rats underwent left anterior descending coronary artery (LAD) ligation, followed by histopathological examination, biochemical assay, and Western blot analysis to evaluate the efficacy and feasibility of Magea13 in AMI. Meanwhile, the Magea13-overexpressing rat cardiomyocyte cell line (H9c2) was also subjected to hypoxia-glucose deficiency/reperfusion to mimic AMI injury to further validate its effects in vitro.

Results The cardiomyocyte-specific overexpression of Magea13 was observed to attenuate myocardial injury in rats with acute myocardial infarction. Furthermore, Magea13 overexpression was demonstrated to attenuate OGD/R-induced H9c2 cell injury. Mechanistic studies have suggested that the protective effect of Magea13 may be mediated through the cAMP-PKA pathway.

Conclusion Magea13 has been demonstrated to offer protection against AMI myocardial injury through the cAMP-PKA signaling pathway and is therefore a promising therapeutic and predictive target for AMI myocardial injury.

Keywords Apoptosis · Acute myocardial infarction · Magea13 · cAMP-PKA pathway

Introduction

Acute myocardial infarction (AMI) is a serious cardiovascular condition primarily caused by the rupture and erosion of unstable plaques associated with coronary artery disease [1]. These pathological changes can induce thrombosis, reducing blood flow to the coronary arteries, which leads to prolonged myocardial ischemia and ultimately triggering myocardial cell necrosis [2]. According to the American Heart Association, the overall prevalence of AMI is approximately 3%. Although significant progress has been made in the treatment of AMI, significant challenges remain in reversing myocardial injury, inhibiting post-injury myocardial remodeling, and reducing the incidence of adverse cardiovascular events after surgery [3, 4]. Therefore, it is clinically important to explore new biomarkers to enhance the diagnosis and treatment of AMI.

Cyclic adenosine monophosphate (cAMP) / protein kinase A (PKA) pathway plays an important role in the progression of AMI. This signaling cascade is critical for a variety of cellular processes, including cardiac contractility, metabolism, and gene expression, all of which are significantly affected during AMI. Activation of cAMP/PKA pathway enhances cardiac function and protects against ischemic injury. For example, it has been shown that inhibition of adenylyl cyclase type 5, which is involved in cAMP synthesis, prevents levodopa-induced

✉ Hualei Dai
dhleitg@163.com

[1] Department of Cardiology, Fuwai Yunnan Hospital, Chinese Academy of Medical Sciences/Affiliated Cardiovascular Hospital of Kunming Medical University, Kunming city, Yunnan Province 650102, China

[2] Department of Cardiology, The Second People's Hospital of Yunnan Province/Affiliated Hospital of Yunnan University, No.176 Qingnian Road, Wuhua District, Kunming city, Yunnan Province 650021, China

dyskinesia in an animal model, further emphasizing the importance of cAMP signaling in maintaining cardiac health [5]. In addition, the cAMP/PKA pathway is involved in regulating mitochondrial function and neuronal development, suggesting that its dysregulation may be associated with pathophysiological processes in heart disease [6]. In the context of myocardial infarction, the cAMP/PKA signaling pathway is known to regulate the inflammatory response and apoptosis, both of which are important factors contributing to the progression of cardiac injury following ischemic events [7]. Furthermore, the observation that interactions between the cAMP signaling pathway and other pathways, such as the JAK/STAT pathway, affect cell survival and apoptosis has been demonstrated in various contexts, including multiple myeloma [8]. This highlights the potential of targeting the cAMP/PKA pathway as a therapeutic strategy to mitigate the adverse effects of acute myocardial infarction and improve myocardial prognosis. In conclusion, the cAMP/PKA pathway is a key signaling mechanism that influences the development of acute myocardial infarction through its regulation of cardiac function, inflammation, and cell survival.

MAGE-A (melanoma-associated antigens-a) belongs to the MAGE superfamily, whose members include MAGE-A1-MAGE-A13, and its coding genes are all located on the X chromosome [9, 10]. Studies have shown that Magea13 is aberrantly expressed in a variety of tumors, including breast cancer, and its expression is associated with aggressive tumor characteristics and poor prognosis [11, 12]. In addition to breast cancer, Magea13 has also been associated with other malignancies, including squamous cell carcinoma of the larynx, where its expression correlates with clinical stage and lymph node metastasis [13]. Frequent expression of Magea13 in different cancer types highlights its potential as an immunotherapeutic target, as it is classified as a cancer/testis antigen, which is usually expressed in tumors [14]. To date, no studies have reported on the role of Magea13 in cardiovascular diseases. In an earlier phase of this study, transcriptome sequencing revealed a significant reduction in Magea13 expression in the myocardial tissue of mice with acute myocardial infarction (AMI). Based on this critical observation, this study aims to further investigate the specific role and underlying mechanisms of Magea13 in AMI. In this study, we aimed to elucidate the potential role and molecular basis of Magea13 in AMI through both in vitro and in vivo experimental studies.

Materials and methods

Animals

32 SPF grade SD rats (10 weeks old, 300–350 g, half male and half female), were supplied by SPEF (Beijing) Biotechnology Co. Ltd. They were housed at room temperature of 20–26℃, relative humidity of 40-70%, 12 h of alternating light and dark, well ventilated, fed with pellet diet and free access to water.

Acute myocardial infarction rat model

All rats were acclimatized for 1 week prior to modeling. Preoperative preparation: Rats were fasted for 12 h prior to surgery. The rats were placed in an anesthetic induction box and anesthesia was induced by the administration of 5% isoflurane, and anesthesia was confirmed by the absence of resistance and stable respiration. Surgical operation: The hair on the chest and neck of the rats was shaved off with a pair of scissors and the rats were then placed on a fixation plate. A small amount of depilatory cream was applied to the chest and neck of the rats with a cotton bud, and the hair was evenly applied back and forth, and wiped clean with an alcohol cotton ball. A longitudinal incision of about 1 cm was made with scissors at the lower end of the mandible, and the rat's neck muscles were gradually and bluntly separated with forceps to expose the trachea, and then a gavage needle was slowly inserted into the rat's trachea from the oral cavity, and the gavage needle was secured after the needle was observed through the neck incision. The air outlet of the anesthesia machine was connected to the air inlet of the ventilator, and the isoflurane concentration was adjusted to 3% for maintenance anesthesia, and then the ventilator was turned on.

A longitudinal incision of about 1.5 cm was made with scissors from the skin at the left edge of the sternum, and a 4−0 suture was prepared for the purse-string suture at the incision site. The chest muscles were bluntly separated layer by layer using forceps and hemostatic forceps, and entry into the thoracic cavity was quickly achieved through the 3rd or 4th intercostal space. The rib gap was opened up with hemostatic forceps, and the pericardial membrane was carefully torn away. The heart was gently squeezed with the left hand in conjunction with heartbeat to facilitate its emergence from the orifice. In the line between the lower edge of the left auricle and the conus of the pulmonary artery, the anterior descending branch of the coronary artery was ligated with a 6−0 suture, ensuring appropriate tightness to control the depth of the needle. After ligation, the heart was gently returned to the thoracic cavity, and the air was expelled by squeezing the thoracic cavity and tightening the sutures at the ligature incision, after which the rats were placed on a thermostatic pad until awakening.

To investigate the effect of Magea13 on acute myocardial infarction, the corresponding group of SD rats was

injected with AAV9 vector carrying Magea13 overexpression and its control (Han Biotechnology, China) at a dose of 1011 vg/one via the tail vein 1 week before surgery. A myocardial infarction model was created by ligating the left anterior descending coronary artery (LAD) with a 7/0 silk suture. The sham-operated group used the same experimental steps but did not perform the ligation part.

Myocardial infarction size observed by TTC staining

One week after completion of the modeling, a jugular vein puncture was performed at the end of reperfusion, and a venous puncture indwelling catheter was placed. Twenty mL of 10% TTC solution was injected into the jugular vein; the heart was removed after 10 min, washed with saline, and cut into circular slices of equal thickness along the apical to basal part of the heart in transverse section and fixed in formaldehyde solution for 24 h. Photographs were taken, and the area of myocardial infarction was analyzed and calculated using ImageJ software.

HE staining

A small piece of myocardial tissue was removed and fixed with 4% paraformaldehyde solution for 48–72 h. After repeated rinsing with ultrapure water, the tissue underwent paraffin embedding, sectioning, haematoxylin and eosin staining. Finally, the pathological damage was observed by light microscopy.

Masson staining

Myocardial tissue was fixed with 4% PFA and embedded in paraffin. Paraffin sections were deparaffinized and hydrated. Sections of 5 mm thickness were fixed with 4% PFA and then stained with Masson's trichrome according to the manufacturer's instructions (Servicebio, China). Images were captured using a Nikon Eclipse microscope (Nikon, Japan) and analyzed using NIS Elements (Nikon). Collagen volume fraction (CVF) was analyzed using ImageJ software and was calculated as fibrotic area/total myocardial area.

CK-MB and cTn I level detection

CK-MB and cTn I levels in rat myocardial tissue were measured using the rat creatine kinase isoenzyme MB (CK-MB) ELISA kit (E-EL-R1327, elabscience) and the rat cardiac troponin I (cTn-I) ELISA kit (E-EL-R1253, elabscience). The procedure was performed according to the manufacturer's instructions.

RNA seq

Myocardial samples were collected from sham ($n=3$) and AMI ($n=3$) rats for transcriptome analysis by RNA sequencing. Total RNA was extracted from the tissue samples using Trizol (Invitrogen, USA), and the concentration and purity of RNA was determined using Nanodrop2000. RNA integrity was measured by agarose gel electrophoresis and Agilent 2100 Bioanalyzer. mRNA library construction and high-throughput Illumina sequencing were contracted to Shanghai Parseno Bio-technology Co. Ltd.

DESeq was used to analyze the differential expression of genes, and the ploidy of differential expression and the *P*-value of each gene were calculated. The results of differential expression analysis were screened, and the conditions for screening the differentially expressed genes were: ploidy of expression|log2FoldChange|>1, significance *P*-value < 0.05, and the screened set of significant differential genes were statistically analyzed, and histograms were made for the differential genes between different comparison groups, and the number of up-regulated differential genes and down-regulated differential genes in each comparison group were counted. Volcano plots of differentially expressed genes were drawn using the R language ggplots2 software package. GO enrichment analysis was performed using topGO, which analyzed the gene list and the number of genes for each term using the GO term annotated differential genes, and then calculated the *P*-value by the hypergeometric distribution method (the criterion for significant enrichment is *P*-value < 0.05) to find out the GO terms that were significantly enriched in differentially expressed genes as compared to the whole genome background, thereby identify the major biological functions exercised by the differential genes. KEGG enrichment analysis was performed using clusterprofiler, in which the gene list and number of genes per pathway were calculated using the KEGG pathway annotated differential genes, and then the *P*-value was calculated by the hypergeometric distribution method (the criterion for significant enrichment is *P*-value < 0.05) to find out the K-values that were significantly enriched in differential genes compared with the whole genomic background. The *P*-value was then calculated by the hypergeometric distribution method (the criterion of *P*-value < 0.05) to identify the KEGG pathways that were significantly enriched for the differential genes compared to the whole genomic background, and thus to determine the major biological functions exercised by the differential genes.

Immunohistochemistry

Myocardial tissue was fixed in 4% PFA and embedded in paraffin. Paraffin sections were dewaxed and hydrated.

Sections of 5 mm thickness were fixed in 4% PFA and subjected to citrate buffer antigen retrieval after baking, dewaxed and hydration. After antigen retrieval with 5% BSA, sections were incubated with rabbit anti-Magea13 antibody and Olr649 antibody (1:100) for primary antibody followed by horseradish peroxidase-labelled goat anti-rabbit secondary antibody (1:100) overnight at 4°C. The sections were stained with DAB, counterstained with hematoxylin and rinse, dehydrated, cleared and then sealed for microscopic visualisation.

Cell culture

The H9c2 rat cardiomyocyte cell line (catalogue no. CL-0089) was purchased from Punosai Life Science and Technology Co. Ltd. (Wuhan, China) and cultured in H9c2 cell-specific medium (catalogue no. CM-0089, Punosai) at 37˚C and 5% CO_2 humidity.

Cell transfection

Lentiviral vectors corresponding to rat Magea13 overexpression and their controls were purchased from He Yuan Bio Co. Ltd. H9c2 cells (5×10^5) were inoculated into 6-well plates and cultured for 24 h according to the manufacturer's instructions. When the cells reached 80% confluence, viral solution was added to each well containing cells and medium. Transfected cells were incubated for 24 h at 37 °C in a CO_2 incubator for subsequent experiments.

OGD/R cell model

Magea13-overexpressing lentiviral vectors and their controls were transfected into H9c2 cells 24 h prior to OGD intervention. For OGD/R experiments, when the transfected H9c2 cells reached 80% confluence, the medium was replaced with glucose-free DMEM medium, and the cells were incubated in an anaerobic chamber (95% N_2 and 5% CO_2) at 37˚C for 4 h. The cells were then incubated in normoxic conditions (95% air and 5% CO_2) with normal medium at 37˚C for the indicated time of 6 h as reperfusion. Untreated cells were used as controls.

CCK-8 assay

Cell viability assays were performed using the Enhanced Cell Viability Assay Kit (CCK-8, E-CK-A362, Elabscience) according to the manufacturer's instructions. Briefly, H9c2 cells were inoculated into 96-well plates at a density of 1×10^4 cells/well. After treatment, 10 µl of CCK-8 solution was added to each well and incubated at 37˚C for 2 h. Absorbance was measured at 450 nm using a microplate reader (Bio-Rad Laboratories, Inc.) to calculate the number of viable cells.

Cell apoptosis

Apoptosis was detected using the Annexin V-FITC/PI Apoptosis Kit (E-CK-A211, Elabscience). 1×10^6 cells were collected, centrifuged with PBS at 1500 rpm for 3 min, and washed twice; cells were resuspended by adding 300 µl of pre-cooled 1×Annexin V-FITC conjugate, and 5 µl of Annexin V-FITC and 10 µl of PI were added to each well. 5 µl of Annexin V-FITC and 10 ul of PI were added to each well; after gentle mixing, the cells were incubated for 10 min at room temperature, avoiding light, and then detected by flow cytometry.

TUNEL staining

Cardiomyocyte apoptosis was detected using the TUNEL apoptosis detection kit (E-CK-A322, Elabscience). Cardiomyocytes, or myocardial tissue, were stained by adding TUNEL solution for fixation or sectioning, and then DAPI was added for nuclear staining; TUNEL-stained positive cells were apoptotic cells, and the apoptosis rate was expressed as the number of TUNEL-stained positive cells/total number of cells.

Intracellular Ca^{2+} measurement

Intracellular Ca^{2+} levels were determined using a Fluo-4 calcium fluorescence assay kit (E-BC-F100, Elabscience). Briefly, after exposing the cells to hypoxic conditions, the medium was removed, and the cells were washed three times with phosphate-buffered saline (PBS). 500 µL Fluo-4 AM (final concentration of 1 µM) was added to PBS at 37˚C for 30 min and observed using an inverted fluorescence microscope (Olympus CKX53).

cAMP level assay

Cell samples or rat myocardial tissue were collected and cAMP in cell samples or rat myocardial tissue was measured using the cyclic adenosine monophosphate (cAMP) enzyme-linked immunosorbent assay kit (E-EL-0056, Elabscience) according to the manufacturer's instructions and expressed as pg/ml.

Reverse transcription quantitative polymerase chain reaction (RT-qPCR)

Total RNA was extracted from H9c2 cells after the indicated treatments using TRIzol reagent (R0016, Beyotime)

following the indicated treatments. qPCR assays were performed using the Taqman One-Step Fluorescent Quantitative PCR Kit (T2210, Solarbio). Amplification conditions were as follows: 95˚C for 10 min, followed by 40 cycles of 10 s at 95˚C and 60 s at 60˚C each. Reactions were performed on a quantitative PCR instrument, Thermal Cycler Dice™ Real Time System III (Takara). The mRNA levels were calculated using the $2^{-\Delta\Delta Cq}$ method. Normalisation was performed with GAPDH. The primers used are shown in Table 1 below:

Western blot

H9c2 cells or rat myocardial tissue homogenates were collected and lysed in RIPA-containing buffer (R0010, Solarbio) for 15 min on ice. Lysates were centrifuged at 12,000 g for 15 min and the supernatant was collected. Protein concentration was determined using the BCA Protein Concentration Assay Kit (PC0020, Solarbio). A total of 15 µg of protein was separated by 10% or 12.5% sodium dodecyl sulfate-polyacrylamide gel electrophoresis (SDS-PAGE) and transferred to a polyvinylidene fluoride membrane. The membranes were sealed and then incubated overnight at 4˚C with primary antibodies against Bax, Bcl-2, cleaved caspase-3, PKA, p-PKA, and β-actin. The membranes were then washed with Tris-buffered saline containing Tween 20 and incubated with HRP-conjugated secondary antibodies for 1 h at room temperature. The bands were visualized using a chemiluminescence system (Bio-Rad), and the intensity of the bands was quantified using ImageJ software.

Statistical analysis

Data are expressed as mean ± SD of three independent experiments. Results were compared by one-way ANOVA followed by least significant difference post hoc test using SPSS 22.0 software (SPSS, Inc.). $p < 0.05$ was considered to indicate a statistically significant difference.

Table 1 Primer sequence

Gene		Sequence(5“, →3“)
Magea13	Forward Primer	ATGTGCTCAGTGTCGTTGGT
	Reverse Primer	TCACTGTTGGGTATAGGCTGG
Olr649	Forward Primer	AGATGTTGCTGGGAACATGGG
	Reverse Primer	GGCAAGTTTCAGTACAGGGTG
Bpifa1	Forward Primer	AACTTCGCAAATGCTCTCAGTG
	Reverse Primer	ATTGGAACTGCCTCCTCCAGA
Clca1	Forward Primer	CACCGAGCACATAGGAGCAT
	Reverse Primer	CCTGTCTTGTGGGCCATACT
muc5b	Forward Primer	TGCCCTGATGTGTCCAACTG
	Reverse Primer	CCTCAAGACGGTTGGGTTGA
GAPDH	Forward Primer	GTGGAGTCTACTGGCGTCTT
	Reverse Primer	TGCTGACAATCTTGAGGGA

Results

Construction of rat model of acute myocardial infarction

A rat myocardial infarction model was established through ligation of the anterior descending branch of the coronary artery. The rats were anesthetized and sacrificed one week after the surgery, followed by the collection of heart tissues. Myocardial ischemia was evaluated by TTC staining, and the pathological alterations and the degree of fibrosis of myocardial tissue were analyzed by HE staining and Masson's staining. Additionally, the levels of CK-MB and cTn I, which are markers of myocardial injury in rats, were determined by ELISA.

The results of TTC staining (Fig. 1A-B) indicated that the infarct area in the AMI group was significantly larger than that in the sham group. The results of HE staining (Fig. 1 C-D) demonstrated that the myocardial tissue of the Sham group was structurally intact, with neatly aligned myocardial fibers, no inflammatory cell infiltration, and no cell necrosis. In contrast, the AMI group exhibited disorganized myocardial fibers, with loosened and broken fibers, accompanied by obvious cardiomyocyte hypertrophy and massive inflammatory cell infiltration and cell necrosis. The results of Masson's staining (Fig. 1E-F) revealed that only a small amount of collagen was deposited in the sham group, while a large number of blue collagen fibers were deposited in the myocardial tissue of the AMI group. The ELISA (Fig. 1G-H) results also indicated that the levels of CK-MB and cTn I in the myocardial tissue of rats in the AMI group were significantly higher than those in the Sham group.

Magea13 is lowly expressed in myocardial tissues of rats with acute cardiac machine infarction

Tissue samples were also collected from rats in both the sham and AMI groups, and differentially expressed genes in myocardial tissue of the two groups were evaluated by high-throughput mRNA sequencing (Fig. 2A). We employed the Pearson correlation coefficient to indicate the correlation of gene expression levels among samples; the closer the correlation coefficient is to 1, the greater the similarity of expression patterns among samples. Generally, correlation coefficients ranging from 0.8 to 1 were regarded as very strong correlations; if the correlation coefficient between biological replicates was less than 0.8, the correlation among samples was considered to be low. The results (Fig. 2B) demonstrated that the correlation coefficients among the samples were above 0.96, indicating a high degree of similarity in their expression patterns. Compared with the Sham group, a total of 2985 differentially labeled

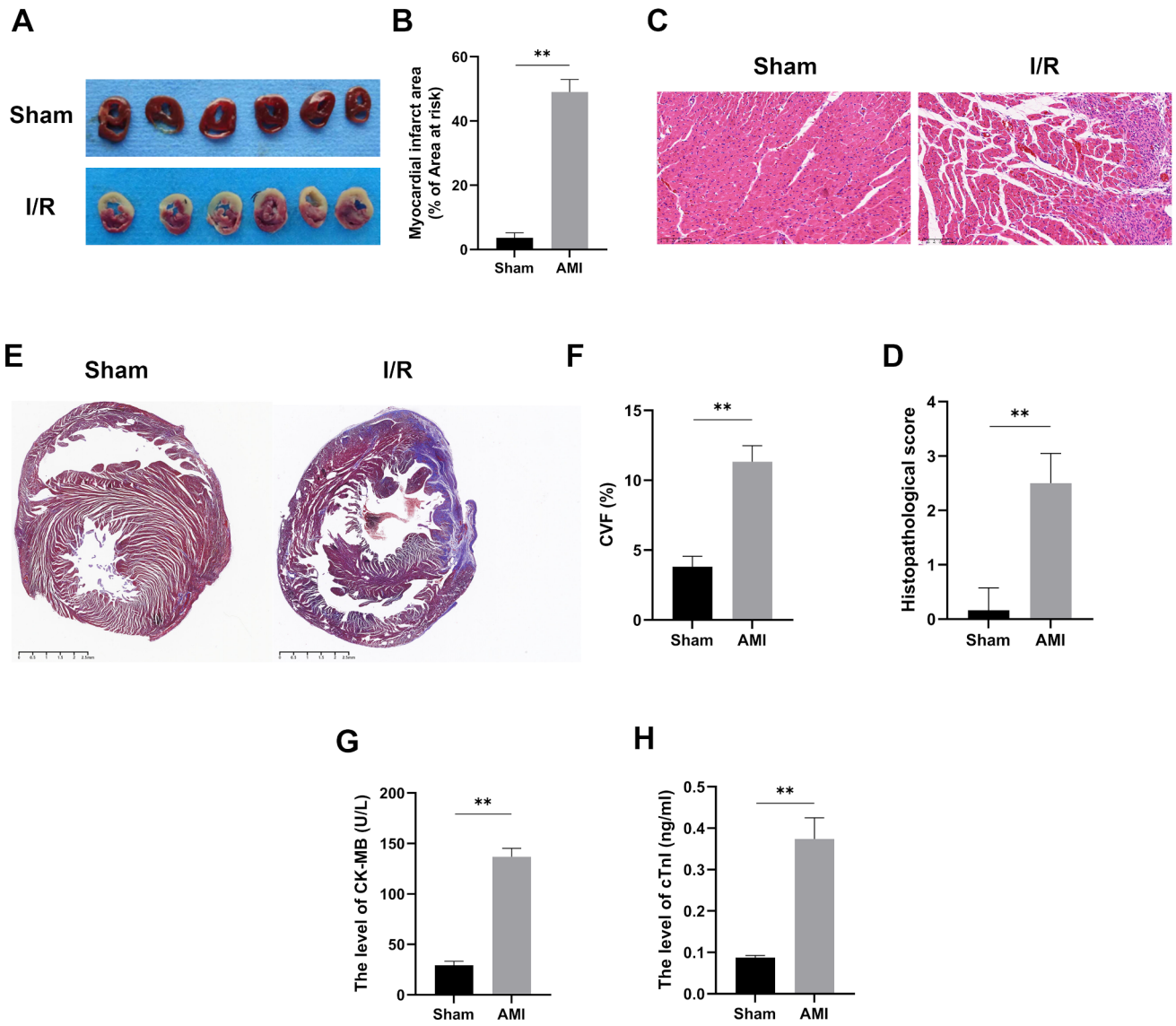

Fig. 1 Construction of rat model of acute myocardial infarction. (**A**) TTC staining of rat myocardial tissue, (**B**) percentage of myocardial ischemic area. (**C**) HE staining of rat myocardial tissue (scale bar, 100 μm), (**D**) Histopathological score of HE staining. (**E**) Masson staining of rat myocardial tissue (scale bar, 2.5 mm), (**F**) Collagen volume fraction. (**G**) CK-MB and (**H**) cTn I level in rat myocardial tissue. **P*<<0.05, ***P*<<<0.01. AMI, Acute myocardial infarction; CK-MB, Creatine Kinase-MB; cTn I, Cardiac Troponin I

genes were detected in the AMI group, among which 2275 were upregulated genes and 710 were downregulated genes (Fig. 2 C).

To determine the functions of the DEGs, we carried out GO term annotation encompassing Molecular Function (MF), Cellular Component (CC), and Biological Process (BP). The results of this GO annotation analysis (Fig. 2D) indicated that the principal GO terms encompassed protein binding, movement of cell or subcellular component, development of anatomical structure, localization, and development of multicellular organism. Meanwhile, KEGG pathway annotation of DEGs between the two groups (Fig. 2E) disclosed that the major pathways included cytokine-cytokine receptor interaction, calcium signaling pathway, and cAMP signaling pathway.

Figure 2 F depicts the expression heatmap of the 15 DEGs with the most pronounced differential expression in myocardial tissue from AMI rats. Based on the maximum and minimum $\log_2$(fold change) values, two of the downregulated genes and three of the upregulated genes were further analyzed. These two downregulated genes were Magea13 (MAGE family member A13) and Olr649 (olfactory receptor family 4 subfamily S member 2, Or4s2), while the three upregulated genes were Bpifa1 (BPI fold-containing family A member 1), Clca1 (calcium-activated chloride channel regulator 1), and Muc5b (mucin 5B, oligomeric mucus/

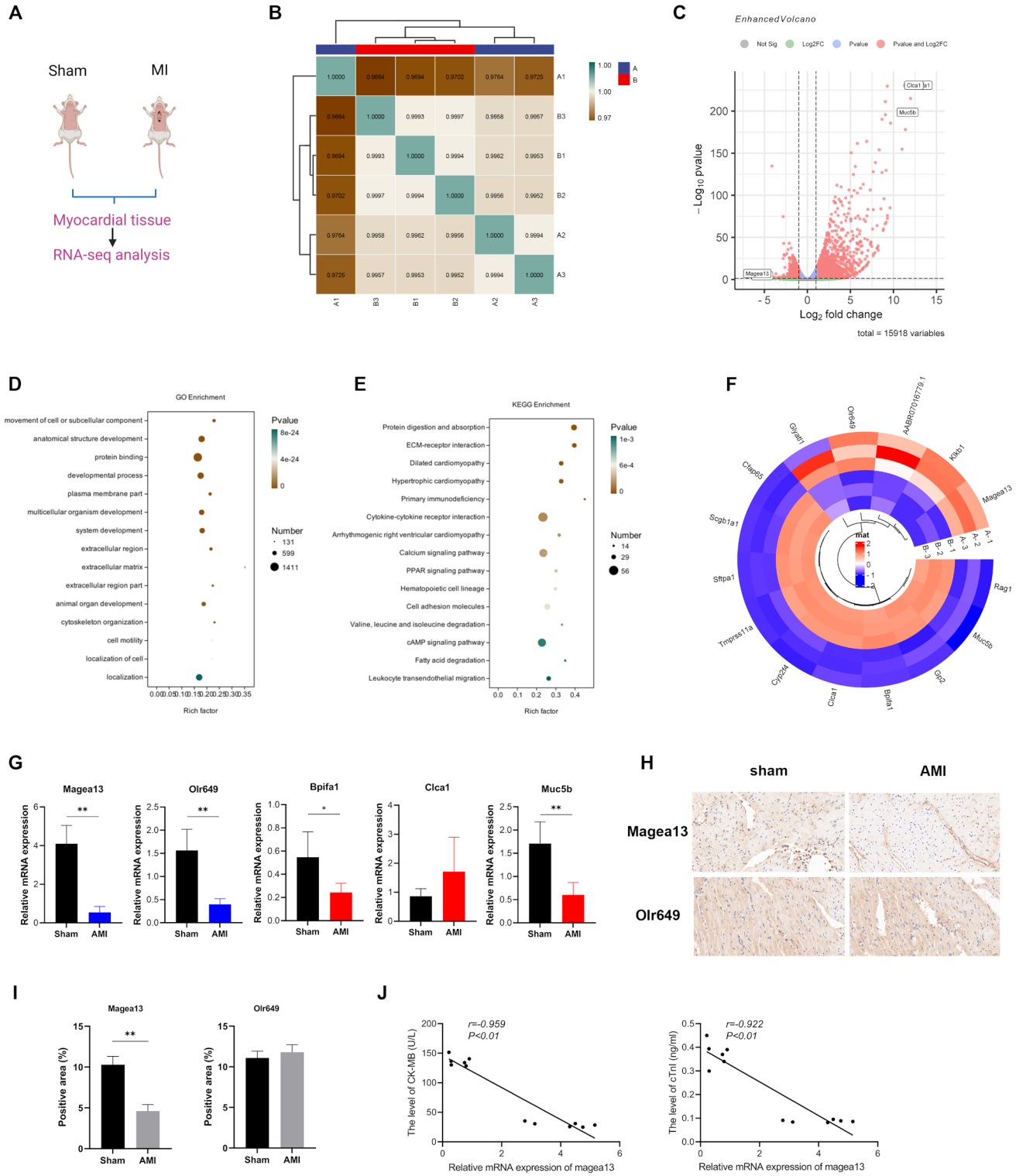

Fig. 2 Magea13 was down-regulated in myocardial tissue of rats with acute myocardial infarction. (**A**) Schematic protocol for RNA-seq. (**B**) Correlation analysis between samples. A: Sham group, B: AMI group. (**C**) Volcano map of significantly different genes in the myocardial tissues from rat in sham and AMI groups based on RNA-seq analysis. (**D**) GO analysis of RNA-seq. (**E**) KEGG analysis of RNA-seq. (**F**) The expression heat map of 15 DEG with the most significant difference expression. (**G**) Relative mRNA levels of Magea13, Olr649, Bpifa1, Clca1 and Muc5b in the myocardial tissues from rat in sham and AMI groups. (**H-I**) The expression of Magea13, Olr649 protein in the myocardial tissues detected by immunohistochemistry. (**J**) Correlation analysis between the relative expression of Magea13 and myocardial injury indexes. **P*<<<0.05, ***P*<<<0.01. AMI, Acute myocardial infarction; CK-MB, Creatine Kinase-MB; cTn I, Cardiac Troponin I

gel-forming). The expression of the above five genes in the myocardial tissue of rats from the sham and AMI groups was further assessed by qPCR assay. The results demonstrated that the levels of Magea13 and Olr649 mRNA were significantly decreased in the myocardial tissues of the AMI group compared to those of the Sham group; concurrently, the levels of Bpifa1 and Muc5b mRNA were also significantly decreased in the myocardial tissues of the AMI group, whereas no significant difference was detected in the levels of Clca1 mRNA (Fig. 2G). The qPCR assay results indicated that only the expression of Magea13 and Olr649 was consistent with the high-throughput sequencing results. Therefore, we further evaluated the expression of Magea13 and Olr649 proteins in the myocardial tissues of rats from the sham and AMI groups by immunohistochemistry. The results revealed (Fig. 2H-I) that the expression level of Magea13 protein in the myocardial tissue of rats in the AMI group was significantly reduced compared with that in the Sham group, whereas no significant alteration in the expression level of Olr649 protein was observed. We also analyzed the correlation between Magea13 mRNA levels and the direction of myocardial injury markers CK-MB and cTn I levels by Pearson correlation coefficient. Scatter plots and correlation analysis disclosed that the relative expression of Magea13 was correlated with myocardial injury markers, with its mRNA level negatively correlated with CK-MB (r=-0.959) and negatively correlated with both cTnI levels (r=-0.922). The aforementioned results suggest that the low expression of Magea13 in rats with an acute myocardial infarction model may be intimately related to the developmental process of AMI.

Magea13 inhibits OGD/R-induced H9C2 cell injury in rat cardiomyocytes

The Magea13 overexpression lentiviral vector was first transfected into H9C2 cells, and the transfection effect of the virus was observed by immunofluorescence, which showed that the fluorescence intensity of both the null group (oe-NC) and the Magea13 overexpression group (oe-Magea13) was very strong (Fig. 3A), indicating the success of viral transfection. qPCR was performed to examine the level of Magea13 mRNA in the transfected cells. The results showed that all Magea13 mRNA levels in the oe-Magea13 group were significantly higher than those in the oe-NC group (Fig. 3B). To evaluate the effect of Magea13 on OGD/R-induced H9C2 cell injury, cell proliferation was assessed by CCK-8 assay, and apoptosis was evaluated by flow cytometry and Tunel staining. The results of CCK-8 assay showed that the cell proliferation activity of the OGD/R group was significantly decreased compared with the control group (Fig. 3 C); compared with the OGD/R group, the cell proliferation activity of the OGD/R + oe-Magea13 group was significantly increased.

The results of flow cytometry assay (Fig. 3D-E) showed that the apoptosis rate was significantly higher in the OGD/R group compared with the control group; the apoptosis rate was significantly lower in the OGD/R + oe-Magea13 group compared with the OGD/R group. The results of Tunel staining (Fig. 3F-G) showed that the percentage of Tunel-positive cells was significantly higher in the OGD/R group compared with the control group; and the percentage of Tunel-positive cells was significantly lower in the OGD/R + oe-Magea13 group compared with the OGD/R group. Changes in the expression of apoptosis-related proteins Bax, Bcl-2 and cleaved caspase3 were further analyzed by WB (Fig. 4A-B). Compared with the control group, the cellular Bax and cleaved caspase3 protein expression levels were significantly increased in the OGD/R group, while the Bcl-2 protein expression levels were significantly decreased. Compared with the OGD/R group, the cellular Bax and cleaved caspase3 protein expression levels were significantly decreased in the OGD/R + Magea13 group, while the Bcl-2 protein expression level was significantly increased. The above results suggested that Magea13 could inhibit OGD/R-induced H9C2 cell injury in rat cardiomyocytes.

Magea13 attenuates OGD/R-induced H9C2 cell injury by inhibiting the cAMP/PKA pathway

According to the KEGG annotation results, the cAMP pathway was found to be significantly enriched. Therefore, the present study further investigated the changes in the levels and protein expression of cAMP/PKA pathway-related compounds in H9C2 cells after Magea13 overexpression. We detected changes in intracellular Ca^{2+} levels by immunofluorescence, measured intracellular cAMP levels by ELISA, and analyzed the expression of PKA and p-PKA proteins by Western blot. The results of Ca^{2+} immunofluorescence staining (Fig. 4 C-D) showed that the OGD /R group had a significant increase in cellular Ca^{2+} levels compared with the control group; whereas in the OGD/R + oe-Magea13 group, the Ca^{2+} levels showed a significant decrease in the OGD/R + oe-Magea13 group compared with the OGD/R group. The results of ELISA assay showed (Fig. 4E) that cellular cAMP levels were significantly increased in the OGD/R group compared to the control group. Western blot analysis showed (Fig. 4F-I) that there was no significant difference in PKA protein expression levels among all experimental groups; however, compared with the control group, cellular p-PKA protein expression levels were significantly increased; compared with the OGD/R combination, p-PKA protein expression levels were significantly decreased in both OGD/R + oe-Magea13 combinations. The above results

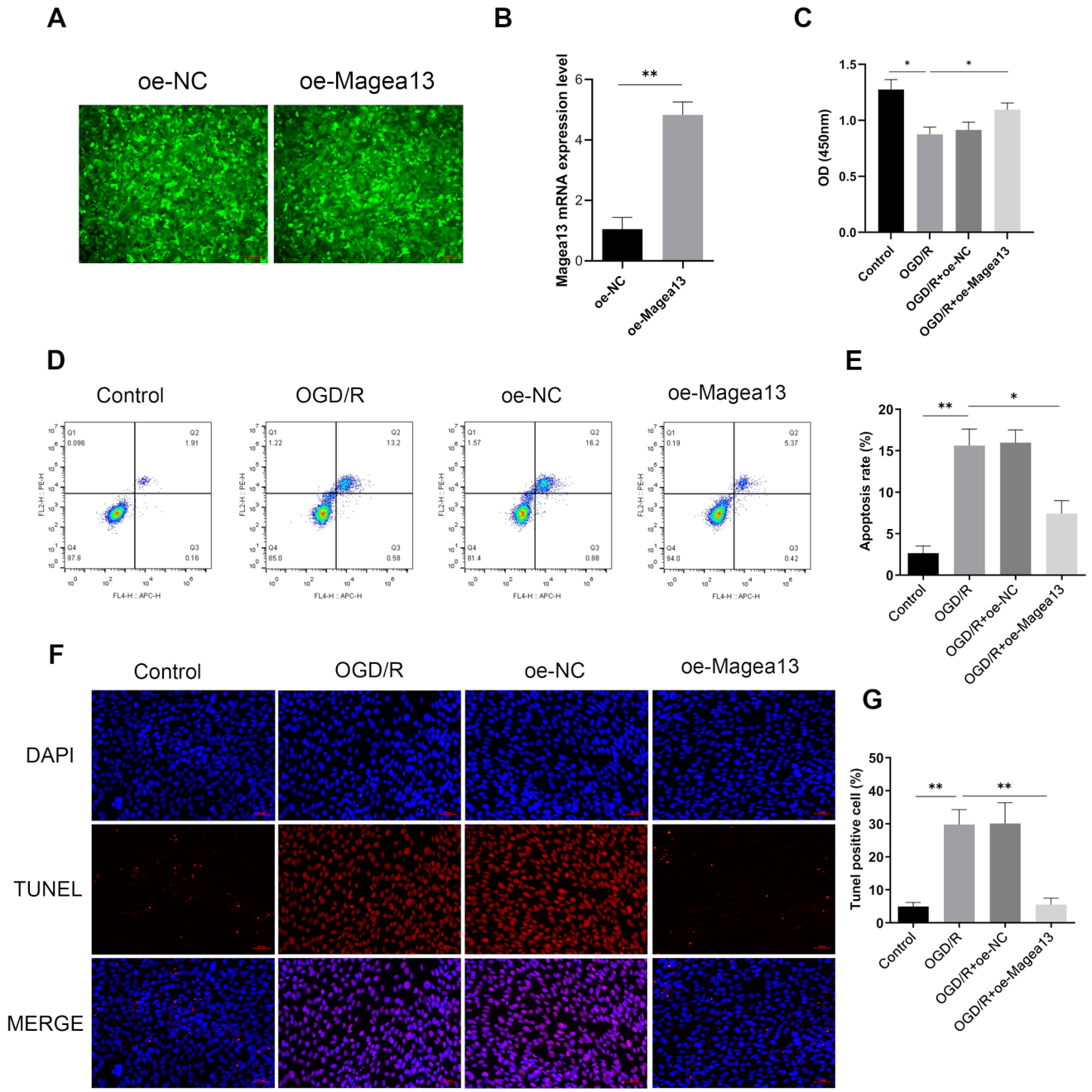

Fig. 3 Magea13 inhibits OGD/R-induced H9C2 cell damage. (**A**) Immunofluorescence observation of the transfection effects of oe-NC and oe-Magea13 lentivirus. (**B**) Relative mRNA levels of magea13 in oe-NC and oe-Magea13 group cells. (**D-E**) The apoptosis rate of H9C2 cell detected by flow cytometry. (**F-G**) The percentage of Tunel positive cell detected by Tunel staining. **P*<<<0.05, ***P*<<<0.01

suggest that Magea13 may attenuate OGD/R-induced H9C2 cell injury by inhibiting the cAMP/PKA signaling pathway.

Magea13 inhibits myocardial injury in rats with acute myocardial infarction

To investigate the role of Magea13 in vivo, we used a constructed Magea13-overexpressing adeno-associated virus (AAV9-Magea13), which was injected into rats by in situ injection to specifically upregulate the level of Magea13 in the rat heart, and assessed its effect on myocardial injury in rats with myocardial infarction. The results of Masson's staining showed (Fig. 5A-B) that the collagen volume fraction (CVF) of rats in the AMI group was significantly higher than that of the sham group; and the CVF of rats in the AMI+AAV9-Magea13 group was significantly lower than

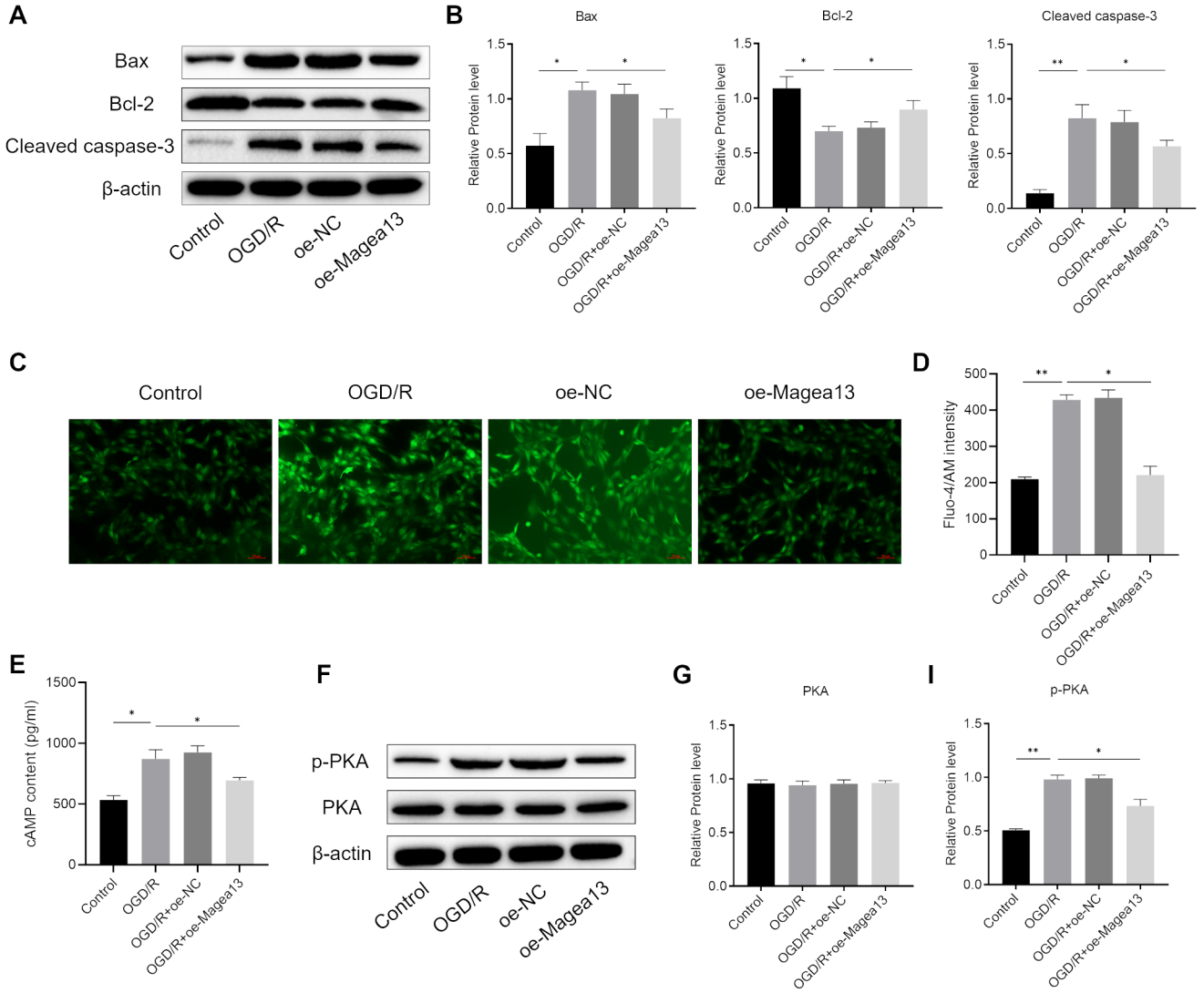

Fig. 4 Magea13 alleviates OGD/ R-induced H9C2 cell damage by inhibiting cAMP/PKA pathway. (**A**) Representative western blot images of Bax, Bcl-2 and Cleaved caspase3. (**B**) Histogram of protein expression of Bax, Bcl-2 and Cleaved caspase3. (**C-D**) The Ca^{2+} content in cells detected by Fluo-4AM fluorescence staining. (**E**) The intracellular cAMP content detected by ELISA. (**F**) Representative western blot images of PKA and p-PKA. (**G-I**) Histogram of protein expression of PKA and p-PKA. **P*<<<0.05, ***P*<<<0.01

that of the AMI group. The results of HE staining showed (Fig. 5 C-D) that the AMI and AMI+AAV9-NC groups had a disorganised, loose and fractured arrangement of cardiac myofibres, accompanied by obvious cardiomyocyte hypertrophy and a large number of inflammatory cell infiltration and cell necrosis, whereas the sham and AMI+AAV9-Magea13 groups showed intact myocardial tissue structure and myocardial fibers were neatly arranged. The ELISA results showed that the levels of CK-MB and cTn I in the myocardial tissue of rats in the AMI group were significantly higher than those in the sham group; compared with the AMI group, the proportion of Tunel-positive cells in rats in the AMI+AAV9-Magea13 group was significantly lower; compared with the AMI group, the levels of cTn I in myocardial tissue of rats in the AMI+AAV9-Magea13 group were significantly lower than those in the sham group. The CK-MB and cTn I levels in the myocardial tissue of rats in the AMI+AAV9-Magea13 group were significantly lower than those in the AMI group. The above results indicated that overexpression of Magea13 could attenuate myocardial injury in AMI rats.

Magea13 may attenuate myocardial injury in rats with myocardial infarction by inhibiting the cAMP/PKA pathway

The results of the above cellular experiments indicated that Magea13 attenuated OGD/R-induced H9C2 cell

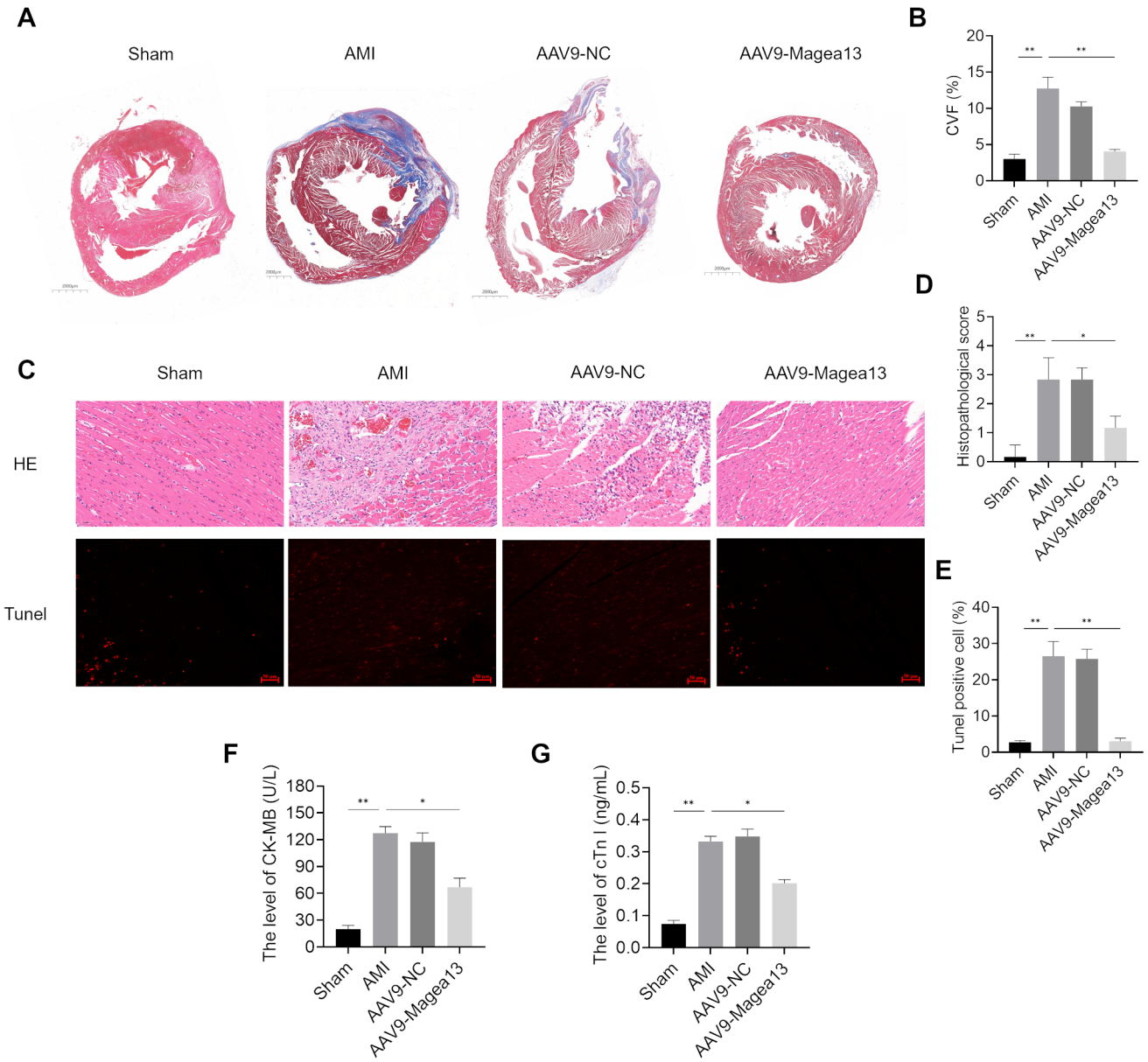

Fig. 5 Magea13 inhibited myocardial damage in rats with myocardial infarction. (**A**) Masson staining of rat myocardial tissue (scale bar, 2.0 mm), (**B**) Collagen volume fraction. (**C**) Above: HE staining of rat myocardial tissue (scale bar, 50 μm); Below: Tunel staining of rat myocardial tissue (scale bar, 50 μm) (**D**) Histopathological score of HE staining. (**E**) Percentage of Tunel positive cells. (**F**) The level of CK-MB in rat myocardial tissue. (**G**) The level of cTn I in rat myocardial tissue. *P<<<0.05, **P<<<0.01

injury, possibly via inhibition of the cAMP/PKA pathway. Therefore, changes in the levels and protein expression of cAMP/PKA pathway-related compounds in myocardial tissue from rats with myocardial infarction were further investigated. Changes in intracellular cAMP levels were detected by ELISA, and changes in cellular PKA and p-PKA protein expression were detected by WB. The results of ELISA showed (Fig. 6A) that cAMP levels were significantly increased in rats in the AMI group compared with the sham group. The results of WB assay (Fig. 6B-D) showed that there was no significant change in PKA protein expression levels in myocardial tissues of rats in each group; p-PKA protein expression levels in rats in the AMI group were significantly increased compared with the sham group; p-PKA protein expression levels in rats in the AMI+AAV9-Magea13 group decreased significantly compared with the AMI group. The above results suggest that Magea13 reduces myocardial injury in rats with myocardial infarction, possibly via inhibition of the cAMP/PKA pathway.

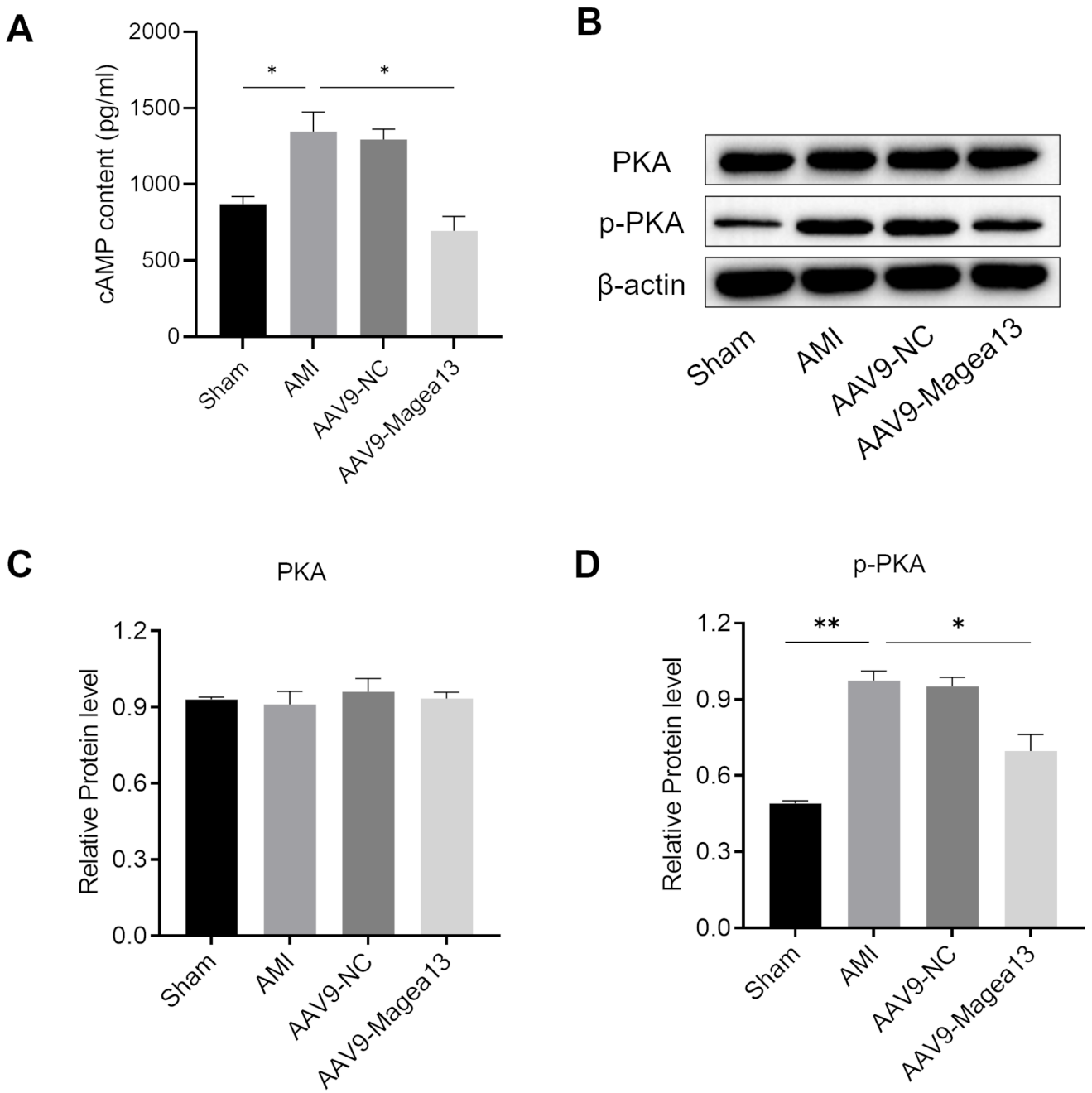

Fig. 6 Magea13 may reduce myocardial damage in rats with myocardial infarction by inhibiting cAMP/PKA pathway. (**A**) The intracellular cAMP content detected by ELISA. (**B**) Representative western blot images of PKA and p-PKA. (**C-D**) Histogram of protein expression of PKA and p-PKA. *P<<<0.05, **P<<<0.01

Discussion

The present study demonstrates, for the first time, that Magea13 expression is significantly reduced in myocardial tissues of rats with AMI. A gain-of-function approach revealed that cardiomyocyte-specific overexpression of Magea13 mitigated myocardial injury in rats with acute myocardial infarction. Moreover, Magea13 overexpression was observed to mitigate OGD/R-induced H9c2 cell injury. The results of the mechanistic studies indicate that the protective effect of Magea13 may be mediated through the cAMP-PKA pathway. Specifically, the efficacy and feasibility of Magea13 in the treatment of AMI were first evaluated in an animal model by replicating a rat model of acute myocardial infarction through anterior descending coronary artery ligation. This model is often used in acute myocardial

infarction studies due to its similarity to human acute myocardial infarction in terms of myocardial ischemia, injury, inflammatory response, and altered cardiac function [15, 16]. Secondly, the therapeutic effect of Magea13 on H9c2 cell injury was evaluated by OGD/R induced H9c2 cell injury model. In light of these findings, we postulate that Magea13 may serve as a promising therapeutic agent against I/R-induced cardiac injury.

Magea13 (melanoma-associated antigen 13) is a protein belonging to the MAGE (melanoma-associated antigens) family, which plays a pivotal role in the immune response, tumorigenesis, and the progression of a multitude of diseases [17]. Initially identified as a tumor-associated antigen in the field of tumor immunology, recent years have seen a growing body of evidence emerge concerning its role in the context of cardiovascular diseases. Magea13 is a cancer germline antigen that has been demonstrated to be associated with the development and progression of a range of cancers. Furthermore, its expression has been shown to correlate with tumor progression and a poor prognosis [18]. Furthermore, Magea13 expression is regulated by DNA methylation and histone deacetylases, indicating that the regulatory mechanisms in the tumor microenvironment may be interlinked with the pathophysiological processes of cardiovascular disease. In the study of cardiovascular diseases, the inflammatory response and immune regulation have been identified as significant pathological mechanisms. It has been demonstrated that specific cytokines, such as IL-37, exert crucial anti-inflammatory effects in the context of cardiovascular disease and may potentially influence the functionality of Magea13 [19]. Furthermore, microRNAs are believed to play a pivotal role in regulating gene expression and intercellular communication, which may influence the expression and function of Magea13 [20]. In conclusion, Magea13 represents a valuable research subject in the field of tumor immunology, and its potential role in cardiovascular disease also requires further investigation. In this study, we employed RNA-seq sequencing to identify the differentially expressed genes in the myocardial tissues of AMI rats and sham-operated control rats. The results demonstrated that Magea13 was markedly under-expressed in the myocardial tissues of AMI rats. This finding was subsequently validated through the use of quantitative polymerase chain reaction (qPCR) and immunohistochemistry. Furthermore, this study revealed a negative correlation between Magea13 mRNA levels and CK-MB and cTn-I levels in myocardial tissues of AMI rats. It can thus be proposed that the low expression of Magea13 may be closely related to the pathological process observed in AMI rats.

It has been demonstrated that OGD/R-induced H9c2 cell injury mimics a number of pathophysiological processes associated with acute myocardial infarction, including ischemia-reperfusion injury, oxidative stress, cell death, the inflammatory response, calcium overload, and mitochondrial damage. These processes have been observed in studies referenced in sources [21–23]. Consequently, the OGD/R model has been extensively employed in the investigation of acute myocardial infarction as an in vitro simulation tool, offering a valuable experimental platform for elucidating the mechanisms of cardiac injury, drug screening, and therapeutic strategies. The present study demonstrated that the overexpression of Magea13 facilitated the proliferation and inhibited the apoptosis of H9c2 cells under OGD/R treatment. Additionally, the overexpression of Magea13 was observed to significantly enhance the expression of Bax and Cleaved Caspase 3 proteins in H9c2 cells, while concurrently reducing Bcl-2 protein levels. These findings suggest that Magea13 may mitigate OGD/R-induced H9c2 cell injury, thereby prompting a comprehensive investigation into the function of Magea13 in AMI.

The role of Magea13 in AMI was subsequently corroborated by an animal model. Magea13 levels were specifically upregulated in rat hearts by injecting it into rats via in situ injection, and its effect on myocardial injury in rats with myocardial infarction was subsequently assessed. The results demonstrated that Magea13 overexpression led to a reduction in collagen volume fraction, an improvement in myocardial histopathology, and a inhibition of cardiomyocyte apoptosis in AMI rats. Additionally, there was a reduction in CK-MB and cTn-I levels in myocardial tissues of rats in the AMI group. These findings suggest that Magea13 may have a protective effect against myocardial injury in AMI rats.

The cAMP/PKA signaling pathway plays a significant role in cardiovascular physiology and is instrumental in regulating cellular function, as well as in cardioprotection following an AMI [24]. cAMP is an intracellular second messenger that transmits signals primarily through the activation of PKA [25]. The pathway is not only involved in the regulation of physiological processes, including cardiac contraction, rhythm, and energy metabolism, but also in the response of cardiomyocytes to ischemia-reperfusion injury. Recent studies have demonstrated the complexity of the role of the cAMP/PKA signaling pathway in AMI. Following AMI, cardiomyocytes are severely threatened due to ischemia and reperfusion injury. The cAMP/PKA signaling pathway plays a dual role in this process, both protective and injury-promoting. In the acute phase of AMI, apoptosis of cardiomyocytes results in a significant reduction in cardiac function. However, the activation of the cAMP/PKA pathway has been demonstrated to attenuate this process and safeguard cardiomyocytes [26]. In the context of ischemia-reperfusion injury, the cAMP/PKA signaling pathway has been demonstrated to confer protection to

cardiomyocytes through the regulation of calcium homeostasis and mitochondrial function [27]. The activation of the cAMP/PKA pathway has been observed to facilitate the pumping of calcium ions, attenuate calcium overload in cardiomyocytes, and reduce the incidence of cell injury and necrosis. A number of studies have demonstrated that elevated cAMP levels assist cardiomyocytes in maintaining metabolic stability and enhancing cell membrane stability, thereby enhancing cardiomyocyte survival [28]. While the cAMP/PKA signaling pathway exerts a protective effect on cardiomyocytes, its over-activation may result in adverse effects. Elevated levels of cAMP can result in an increased excitability of cardiomyocytes, which may subsequently induce arrhythmias. Furthermore, cAMP overactivation has the potential to promote fibrosis in cardiac tissues and influence the cardiac remodeling process [29, 30]. A number of studies have demonstrated that PKA, by enhancing the activity of specific transcription factors, may intensify the structural alterations of the heart following a myocardial infarction, expand the area of fibrotic regions, and precipitate a further deterioration in cardiac function [31, 32]. The findings indicate that moderate activation of the cAMP/PKA pathway may contribute to the attenuation of apoptosis, the promotion of cardiomyocyte survival, and the enhancement of cardiac function following myocardial infarction. However, excessive activation may potentially give rise to arrhythmia and cardiac remodeling complications. The results of this study demonstrated that the cAMP pathway was significantly enriched in accordance with the KEGG annotation results. Furthermore, OGD treatment of H9c2 cells resulted in elevated levels of Ca^{2+} and cAMP, as well as increased levels of PKA protein phosphorylation. However, Magea13 overexpression was observed to reverse these changes in H9c2 cells. Similarly, elevated levels of cAMP and PKA protein phosphorylation were observed in AMI rat myocardial tissues. Furthermore, Magea13 overexpression was observed to reverse these changes in AMI rat myocardial tissues. This indicates that Magea13 may exert a protective effect against apoptosis, enhance cardiomyocyte survival, and improve cardiac function after myocardial infarction by inhibiting excessive activation of the cAMP/PKA pathway. The cAMP-PKA signaling pathway precisely regulates the physiological activities and pathological reactions of cells through a variety of downstream targets and secondary pathways. It not only directly phosphorylates transcription factors (such as cAMP response element binding protein (CREB)), metabolic regulatory factors (such as Glycogen synthase kinase 3β(GSK-3β), lipase HSL) and cyclins, but also mediates cell proliferation, differentiation, survival and metabolism by affecting ion channels, protein synthesis, cell migration and other multiple mechanisms [33–35]. In addition, the cAMP-PKA signaling pathway also profoundly affects the stress response, migration behavior and immune function of cells by regulating non-classical effectors such as the exchange protein directly activates cAMP (EPAC), ERK, etc [36, 37]. However, in this study, the situation of these downstream targets and signaling pathways is not clear and deserves further investigation.

To date, Magea13 has been shown to have myocardial protective potential after myocardial infarction in animal studies. However, the specific expression of Magea13 in patients with acute myocardial infarction (AMI) has not been fully investigated. Therefore, future studies should focus on evaluating the expression level of Magea13 in AMI patients and its association with clinical outcomes. We plan to design a prospective cohort study to collect serum and cardiac tissue samples at different time points, determine the expression level of Magea13 by ELISA and immunohistochemistry, and analyse its correlation with clinical indices (e.g. markers of myocardial injury, cardiac function recovery, etc.).

Conclusion

In conclusion, the present study identified Magea13 as a potential therapeutic agent for AMI and established a correlation between lower Magea13 levels after AMI and poorer outcomes. From a mechanistic perspective, Magea13 may exert a protective effect against apoptosis and promote cardiomyocyte survival following myocardial infarction by inhibiting cAMP/PKA hyperactivation. However, there are some shortcomings in this paper, and the specific performance of Magea13 in patients with AMI has not been fully studied. Therefore, future studies should focus on assessing the expression level of Magea13 in AMI patients and its relationship with clinical outcomes.

Acknowledgements The authors would like to express their gratitude to the participating centers and members.

Author contributions Conceptualization, JL.Z and HL.D; methodology, XY.X; software, XY.X.; validation, ZW.Z, XY.X. and JL.Z; formal analysis, KH.G; investigation, KH.G.; resources, JL.Z; data curation, Y.X; writing—original draft preparation, JL.Z.; writing—review and editing, JL.Z and HL.D; visualization, XY.X; supervision, ZW.Z; project administration, LM.W; funding acquisition, JL.Z and HL.D. All authors have read and agreed to the published version of the manuscript.

Funding This work was supported by grants from The Association Foundation Program of Yunnan Provincial Science and Technology Department and Kunming Medical University (Grant No. 202401AY070001-162) and Reserve talents of young and middle-aged academic and technical leaders of Yunnan (Grant No. 202305AC160076).

Data availability Data and materials may be obtained from the corresponding author upon reasonable request.

Declarations

Ethics approval and consent to participate All experimental protocols were approved by the Animal Experiment Ethics Committee of BST Biotechnology Co., LTD (Approval No. BST-PZ-RAT-20240517-01).

Patient consent for publication The article does not involve clinical patients.

Competing interests The authors declare no competing interests.

References

1. Dauerman HL, Ibanez B (2021) The Edge of Time in Acute myocardial infarction. J Am Coll Cardiol 77(15):1871–1874
2. Barrère-Lemaire S, Vincent A, Jorgensen C et al (2024) Mesenchymal stromal cells for improvement of cardiac function following acute myocardial infarction: a matter of timing. Physiol Rev 104(2):659–725
3. Xue J, Yan X, Yang Y et al (2019) Connexin 43 dephosphorylation contributes to arrhythmias and cardiomyocyte apoptosis in ischemia/reperfusion hearts. Basic Res Cardiol 114(5):40
4. Yu L, Yang G, Zhang X et al (2018) Megakaryocytic Leukemia 1 bridges epigenetic activation of NADPH oxidase in macrophages to Cardiac Ischemia-Reperfusion Injury. Circulation 138(24):2820–2836
5. Park HY, Kang YM, Kang Y et al (2014) Inhibition of adenylyl cyclase type 5 prevents L-DOPA-induced dyskinesia in an animal model of Parkinson's disease. J Neurosci 34(35):11744–11753
6. Dagda RK, Das Banerjee T (2015) Role of protein kinase A in regulating mitochondrial function and neuronal development: implications to neurodegenerative diseases. Rev Neurosci 26(3):359–370
7. Kloster MM, Naderi EH, Carlsen H et al (2011) Hyperactivation of NF-κB via the MEK signaling is indispensable for the inhibitory effect of cAMP on DNA damage-induced cell death. Mol Cancer 10:45
8. Follin-Arbelet V, Torgersen ML, Naderi EH et al (2013) Death of multiple myeloma cells induced by cAMP-signaling involves downregulation of Mcl-1 via the JAK/STAT pathway. Cancer Lett 335(2):323–331
9. Zhang Y, Zhang Y, Zhang L (2019) Expression of cancer-testis antigens in esophageal cancer and their progress in immunotherapy. J Cancer Res Clin Oncol 145(2):281–291
10. Meek DW, Marcar L (2012) MAGE-A antigens as targets in tumour therapy. Cancer Lett 324(2):126–132
11. Xia LP, Xu M, Chen Y et al (2013) Expression of MAGE-A11 in breast cancer tissues and its effects on the proliferation of breast cancer cells. Mol Med Rep 7(1):254–258
12. Lian Y, Sang M, Ding C et al (2012) Expressions of MAGE-A10 and MAGE-A11 in breast cancers and their prognostic significance: a retrospective clinical study. J Cancer Res Clin Oncol 138(3):519–527
13. Liu S, Sang M, Xu Y et al (2016) Expression of MAGE-A1, -A9, -A11 in laryngeal squamous cell carcinoma and their prognostic significance: a retrospective clinical study. Acta Otolaryngol 136(5):506–513
14. Park TS, Groh EM, Patel K et al (2016) Expression of MAGE-A and NY-ESO-1 in primary and metastatic cancers. J Immunother 39(1):1–7
15. Xie S, Xing Y, Shi W et al (2022) Cardiac fibroblast heat shock protein 47 aggravates cardiac fibrosis post myocardial ischemia-reperfusion injury by encouraging ubiquitin specific peptidase 10 dependent Smad4 deubiquitination. Acta Pharm Sin B 12(11):4138–4153
16. Ge S, Wu S, Yin Q et al (2024) Ecliptasaponin A protects heart against acute ischemia-induced myocardial injury by inhibition of the HMGB1/TLR4/NF-κB pathway. J Ethnopharmacol 335:118612
17. Younas K, Quintela M, Thomas S et al (2019) Delayed endometrial decidualisation in polycystic ovary syndrome; the role of AR-MAGEA11. J Mol Med (Berl) 97(9):1315–1327
18. James SR, Cedeno CD, Sharma A et al (2013) DNA methylation and nucleosome occupancy regulate the cancer germline antigen gene MAGEA11. Epigenetics 8(8):849–863
19. Zhuang X, Wu B, Li J et al (2017) The emerging role of interleukin-37 in cardiovascular diseases. Immun Inflamm Dis 5(3):373–379
20. Wang F, Chen C, Wang D (2014) Circulating microRNAs in cardiovascular diseases: from biomarkers to therapeutic targets. Front Med 8(4):404–418
21. Tong Q, Zhu PC, Zhuang Z et al (2019) Notoginsenoside R1 for organs Ischemia/Reperfusion Injury: a preclinical systematic review. Front Pharmacol 10:1204
22. Jiang S, Zhao G, Lu J et al (2020) Silencing of circular RNA ANRIL attenuates oxygen-glucose deprivation and reoxygenation-induced injury in human brain microvascular endothelial cells by sponging miR-622. Biol Res 53(1):27
23. Lin Y, Yang X, Li Y et al (2024) A newly synthesized flavone avoids COMT-catalyzed methylation and mitigates myocardial ischemia/reperfusion injury in H9C2 cells via JNK and P38 pathways. Iran J Basic Med Sci 27(4):492–499
24. Meng L, Lu Y, Wang X et al (2023) NPRC deletion attenuates cardiac fibrosis in diabetic mice by activating PKA/PKG and inhibiting TGF-β1/Smad pathways. Sci Adv 9(31):eadd4222
25. Wu J, Liu B, Mao W et al (2020) Prostaglandin E2 regulates activation of mouse peritoneal macrophages by Staphylococcus aureus through Toll-Like receptor 2, toll-like receptor 4, and NLRP3 Inflammasome Signaling. J Innate Immun 12(2):154–169
26. Gong J, Zhou F, Wang SXX et al (2020) Caveolin-3 protects diabetic hearts from acute myocardial infarction/reperfusion injury through β2AR, cAMP/PKA, and BDNF/TrkB signaling pathways. Aging 12(14):14300–14313
27. Khaliulin I, Bond M, James AF et al (2017) Functional and cardioprotective effects of simultaneous and individual activation of protein kinase A and Epac. Br J Pharmacol 174(6):438–453

28. Takahashi T, Tang T, Lai NC et al (2006) Increased cardiac adenylyl cyclase expression is associated with increased survival after myocardial infarction. Circulation 114(5):388–396
29. Francisco J, Zhang Y, Nakada Y et al (2021) AAV-mediated YAP expression in cardiac fibroblasts promotes inflammation and increases fibrosis. Sci Rep 11(1):10553
30. Landry NM, Dixon IMC (2020) Fibroblast mechanosensing, SKI and Hippo signaling and the cardiac fibroblast phenotype: looking beyond TGF-β. Cell Signal 76:109802
31. He T, Huang J, Chen L et al (2020) Cyclic AMP represses pathological MEF2 activation by myocyte-specific hypo-phosphorylation of HDAC5. J Mol Cell Cardiol 145:88–98
32. Minerath RA, Hall DD, Grueter CE (2019) Targeting transcriptional machinery to inhibit enhancer-driven gene expression in heart failure. Heart Fail Rev 24(5):725–741
33. Yan C, Yang Z, Chen P et al (2024) GPR65 sensing tumor-derived lactate induces HMGB1 release from TAM via the cAMP/PKA/CREB pathway to promote glioma progression. J Exp Clin Cancer Res 43(1):105
34. Chen Z, Zhong Y, Chen J et al (2022) Disruption of β-catenin-mediated negative feedback reinforces cAMP-induced neuronal differentiation in glioma stem cells. Cell Death Dis 13(5):493
35. Abe T, Sato T, Murotomi K (2023) Sudachitin and Nobiletin Stimulate Lipolysis via activation of the cAMP/PKA/HSL pathway in 3T3-L1 adipocytes. Foods.;12(10)
36. Zhang H, Liu Y, Liu J et al (2024) cAMP-PKA/EPAC signaling and cancer: the interplay in tumor microenvironment. J Hematol Oncol 17(1):5
37. Ma J, Hermans L, Dierick M et al (2024) Enterotoxigenic Escherichia coli heat labile enterotoxin affects neutrophil effector functions via cAMP/PKA/ERK signaling. Gut Microbes. Jan-Dec;16(1):2399215